ChemComm

Thermal Properties of Cubic NaSbS2: Diffusion Dominant Thermal Transport Above the Debye Temperature

Journal:	*ChemComm*
Manuscript ID	CC-COM-07-2023-003455.R1
Article Type:	Communication

COMMUNICATION

Thermal Properties of Cubic $NaSbS_2$: Diffusion Dominant Thermal Transport Above the Debye Temperature

Received 00th January 20xx,
Accepted 00th January 20xx

DOI: 10.1039/x0xx00000x

Wilarachchige D. C. B. Gunatilleke,[a] Oluwagbemiga P. Ojo [a] and George S. Nolas *[a]

We elucidate the thermal properties of superionic conductors, which are of intense current interest for solid-state battery applications. The temperature-dependent thermal properties of superionic $NaSbS_2$ were investigated by analyses of appropriate models revealing that a predominant contribution to thermal transport above the Debye temperature is from thermal diffusion.

Chalcogenides have been at the forefront of current materials research due to their physical properties and the numerous avenues for developing novel compositions of interest, as well as the ability to tune the material properties for targeted technological applications. A fundamental understanding of thermal transport of a material is crucial for any application of interest and essential for thermoelectrics, thermal barrier coatings [1–10], phase change materials[11,12] and photovoltaics [13–19]. The thermal properties of novel multinary chalcogenides of diverse structure types have been investigated for these applications[20–26]. Most recently, understanding the thermal properties of solid-state electrolytes has intensified for the development of materials for use in place of liquid electrolytes in Li-ion batteries. This is due to the importance of thermal management in the design and safety of solid-state batteries [27–30]. Among the chalcogenide compositions that are reported as promising solid-state electrolytes, many display superionic conduction as well as low lattice thermal conductivity, κ_L [31–33]. In fact, certain superionic chalcogenide compositions are of interest for thermoelectric applications [34–37].

The relationship between superionic conduction and κ_L has been investigated using the phonon liquid electron crystal (PLEC) concept [36,38,39] as well as diffusion mediated thermal transport [40,41]. Many such investigations involve spectroscopic analyses; however, there are scarce reports on the thermal properties of superionic chalcogenide compositions and the origin of anomalous thermal transport in these materials [28,40,42,43]. The challenge in obtaining dense specimens that are not affected by high humidity may be a reason for the lack of their experimental thermal transport data[27]. Herein, we report on temperature dependent thermal properties of cubic $NaSbS_2$, a material that displays superionic conduction under ambient conditions[44]. This material belongs to a group of polymorphs, of which the monoclinic phase has been investigated as a possible solar absorber material[45–48]. We synthesized phase-pure cubic $NaSbS_2$ ($\boldsymbol{Fm\bar{3}m}$) allowing for temperature-dependent thermal conductivity, κ, and isobaric heat capacity, C_p, measurements. Our investigation of the low temperature κ data revealed a direct correlation between the temperature dependent κ and lattice anharmonicity due to thermal diffusion arising from the ion transport in the material. Thermal diffusion dominates the phonon dynamics above the Debye temperature leading to relatively temperature-independent κ near room temperature. Our investigations will aid in the fundamental understanding of thermal transport in this and other related compositions that display superionic conduction.

Phase-pure microcrystalline cubic $NaSbS_2$ was obtained by ball milling a mixture of $Na_2S.9H_2O$ (98+%, Acros Organics), after heating under a dynamic vacuum, and Sb_2S_3 powder (98%, Acros Organics) combined in a 1:1 stoichiometric ratio. The densification of the obtained microcrystalline powder was performed by Spark Plasma Sintering. Rietveld structure refinement of X-ray diffraction (XRD) measurements was employed to analyze the crystal structure of cubic $NaSbS_2$. Differential thermal analysis (DTA) and thermogravimetric analysis (TGA) under nitrogen gas flow for the as-synthesized powders were performed using a TA Instruments Q600 apparatus. A custom designed radiation shielded vacuum probe was used to measure κ from 30 K to 300 K with 8% maximum experimental uncertainty[49,50]. Room temperature four-point probe resistivity and C_p measurements were performed

[a] Department of Physics, University of South Florida, Tampa, FL 33620, USA

Electronic Supplementary Information (ESI) available: [details of any supplementary information available should be included here]. See DOI: 10.1039/x0xx00000x

employing the Physical Property Measurements System from Quantum Design. The details on the specific measurements as well as the crystal structure are provided in the Supplementary Information (SI).

The crystal structure of cubic $NaSbS_2$ is shown in Figure 1(a). It can be thought of as an ideal face-centered cubic (*fcc*) crystal lattice where Na and Sb occupy the 4*a* octahedral Wyckoff position equally, with all Na/Sb-S bond lengths equal to 2.884 Å. Figure 1(b) shows the experimental, calculated and difference diffraction patterns obtained from Rietveld refinement and the refinement results are provided in Tables S1 and S2. We note Bera *et al.*[51] reported local distortion of the crystal lattice for $LiAsSe_2$ that resulted in determination of the crystallographic space group for the structure to be triclinic P$\bar{1}$ for their NaCl-like structure due to unit-cell averaging effects derived from single crystal XRD structure refinement. Hence, we investigated the possibility that local lattice distortions may exist for cubic $NaSbS_2$. However, from our structural analyses it was apparent that the cubic phase is the only probable phase. We also note that first principles investigations by Hua *et al.*[52] show that the most stable phase of $NaSbS_2$ below room temperature to be the non-distorted $\boldsymbol{Fm\bar{3}m}$ structure.

Thermal stability of $NaSbS_2$ was investigated using DTA and TGA. Upon heating, a phase transition from cubic to monoclinic began at approximately 530 K, with only the monoclinic phase observed above 543 K from analyses of the product by XRD. These observations corroborate the studies done by Xia *et al.*[53] on monoclinic $NaSbS_2$. The densified $NaSbS_2$ was also exposed to ambient conditions for several weeks. No degradation was observed in the material in that time. Hence, the material was deemed an excellent candidate to investigate the thermal properties of a superionic conductor.

Measurement and investigation of heat capacity can help elucidate disorder of the crystal structure that may arise due to the reported superionic conduction for this material, which may also lead to lattice anharmonicity. Low temperature C_p data are shown in Figure 3. Near room temperature, the data approach the Dulong-Petit limit indicating that the majority of acoustic and optic mode frequencies are excited above this temperature. The solid line in the inset of Figure 3 is a low

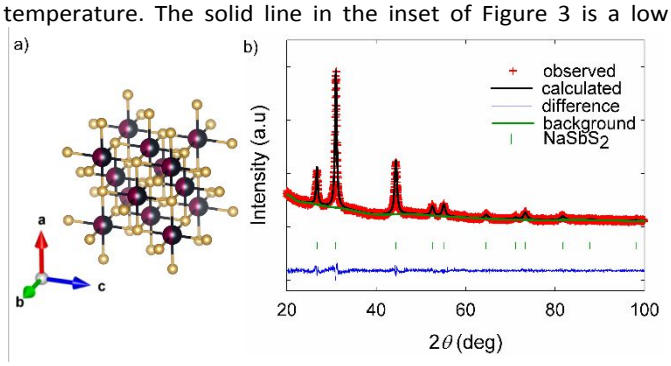

Figure 1 a) The crystal structure of cubic $NaSbS_2$ with Na (red), Sb (black) and S (yellow) forming the face-centered cubic crystal lattice. b) Powder XRD data for $NaSbS_2$, including the profile fit and profile difference from Rietveld refinement.

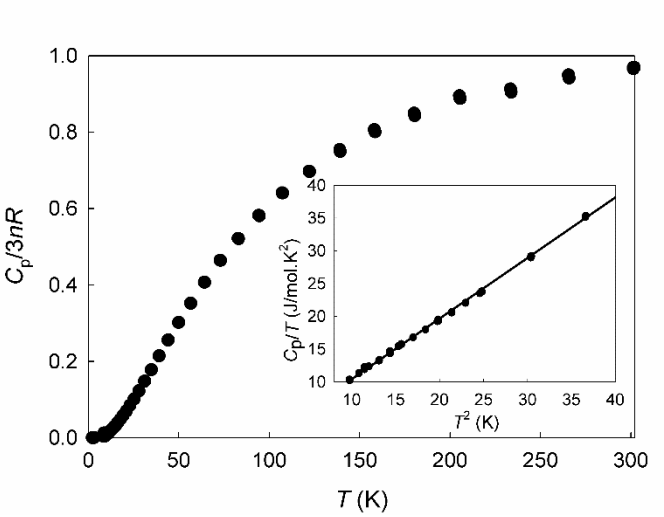

Figure 2. Temperature dependent C_p with the inset showing C_p/T vs T^2 at low temperatures, where the solid line is a fit of the form $C_p/T = \gamma + \beta T^2$.

temperature linear fit to the data of the form $\boldsymbol{C_p = \alpha T + \beta T^3}$, where the first and second terms represent the Sommerfeld coefficient and the lattice contribution, respectively[54]. The low value of the Sommerfeld coefficient, $\boldsymbol{\alpha = 1.45\ mJ\ mol^{-1}K^{-2}}$, indicates a low density of states at the Fermi level, in agreement with the relatively high band gap of 1.3 eV reported for this material[44]. Using the relation $\boldsymbol{\theta_D = (12\pi^4 R n_a/5\beta)^{1/3}}$, $\boldsymbol{\theta_D}$ can be determined from the low temperature C_p data, where $\boldsymbol{n_a}$ is number of atoms per formula unit, and *R* is the universal gas constant. A value of 204 K for $\boldsymbol{\theta_D}$ was thus obtained.

The cubic ordered nature of the crystal structure suggests the material should possess high κ; however, the disorder occurring across the crystal lattice due to mixed occupancy on the 4*a* site by both Na and Sb would result in low κ values. Moreover, we posit that Na^+ ion transport, reported for cubic $NaSbS_2$[44], would presumably result in thermal diffusion. We therefore utilized a phenomenological model in order to understand the different phonon scattering mechanisms affecting thermal transport in this material, where the measured κ was modeled using the Debye-Callaway model, κ_L, combined with the diffusion transport model, κ_{diff} [55,56].

Temperature dependent κ data were utilized for the investigation of the phenomenological model. As shown in Figure 3, $NaSbS_2$ possesses relatively low κ over the entire measured temperature range. The electronic contribution to κ was deemed to be negligible due to very high electrical resistivity values observed for this wide band gap material, with a value of 4.0 kΩ m from our room temperature four-point probe resistivity measurements. Hence, in our model κ is comprised of two terms,

$$\boldsymbol{\kappa = \kappa_L + \kappa_{diff}}, \text{ where} \qquad (1)$$

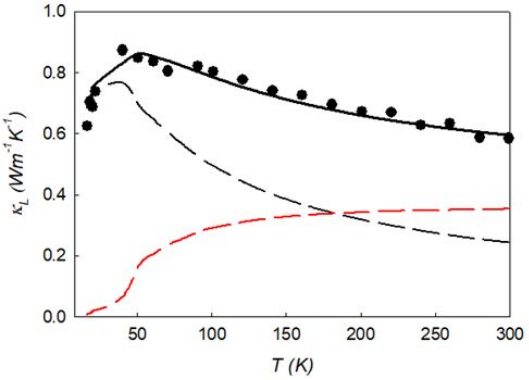

Figure 3. Temperature dependent κ data. The solid line is a fit to the model described in the text with A = 2.4 x 10^{-40} s^3, B = 7.6 x 10^{-17} s/K, υ = 1600 m/s, L = 1 μm, D = 1.0 and f = 1.0. The contributions from thermal diffusion (red dashed line) as well as the lattice (black dashed line) are also shown separately.

$$\boldsymbol{\kappa_L = \frac{k_B}{2\pi^2 v}\left(\frac{k_B T}{\hbar}\right)^3 \int_0^{\theta_D/T} \frac{x^4 e^x}{\tau_C^{-1}(e^x-1)^2} dx} \text{ and} \quad (2)$$

$$\boldsymbol{\kappa_{diff} = \left(\frac{n^{-2/3}k_B}{2\pi^2 v^3}\right)\left(\frac{k_B T}{\hbar}\right)^4 \int_0^{f\theta_D/T} \frac{x^5 e^x}{(e^x-1)^2} dx}. \quad (3)$$

The solid line in Figure 3 represents a theoretical fit to the model. Here $x = \hbar\omega/k_B T$, ω is the phonon frequency, $\hbar$ is the reduced Planck's constant, υ is the average velocity of sound and n is the number of atoms in the unit cell per unit cell volume. The phonon scattering relaxation time, τ_C^{-1}, is given by

$$\boldsymbol{\tau_C^{-1} = \left(\frac{v}{L} + AT^4 x^4 + BT^3 \exp\left(\frac{-\theta_D}{3T}\right) x^2\right)}, \quad (4)$$

where the three terms represent grain boundary scattering, point defect scattering and Umklapp scattering respectively. A and B are fitting parameters related to the different phonon scattering processes, and f is a fitting parameter that was originally used by Agne *et al*.[55] in the diffusion transport model for amorphous Si to achieve agreement with the experimental data. The fitting parameters were uniquely defined using minimization of the best sequence fit function, as compared to the data. To achieve the best data fit, all three terms related to $\boldsymbol{\tau_C^{-1}}$ as well as the expression for κ_{diff} were required. As shown in Figure 3, the model fits the data very well over the entire measured temperature range, with a coefficient of determination, R^2, of 0.96. With increasing temperature, both Umklapp scattering and thermal diffusion contribute to the thermal transport; however, at approximately 200 K thermal diffusion dominates leading to a near temperature independent κ as the temperature approaches room temperature. The relatively low average speed of sound of 1600 m/s obtained from the data fit may be associated with softening of the lattice due to superionic conduction. Softened sheer modes compared to transverse modes resulting in low average speed of sound has been observed in other cubic superionic conductors, for example Cu_2Se[57] and Cu_7PSe_6[58].

To examine the lattice anharmonicity that occurs due to the aforementioned phonon scattering phenomena, the Gruneisen parameter, γ, was calculated. Utilizing the expression for Umklapp scattering used above, specifically the B parameter from the theoretical fit to the phenomenological model, γ = 1.7 was obtained using the expression, $B \cong \hbar\boldsymbol{\gamma^2}/\boldsymbol{Mv^2\theta_D}$ [59]. Anharmonic vibrations have been correlated with materials that exhibit ion transport[34,35,60,61] and the relatively large value of γ is presumably associated with the superionic conduction for this material.

In summary, we investigated the thermal properties of phase-pure cubic $NaSbS_2$ for the first time. Low temperature C_p measurements revealed a $\boldsymbol{\theta_D}$ value of 204 K with low density of states at the Fermi level for this relatively wide band gap material. Analyses of the temperature dependent κ data employing the Debye-Callaway and diffusion transport models indicate that κ_{diff} dominates κ near room temperature. Thermal diffusion leads to lattice anharmonicity in this superionic material. These results will contribute to the fundamental understanding of the thermal properties of materials that display superionic conduction, and help with the development of this as well as other chalcogenides with superionic conduction for solid state battery and thermoelectric applications.

The authors acknowledge financial support from the U.S. National Science Foundation (NSF) under Grant No. DMR-1748188.

Wilarachchige D. C. B. Gunatilleke: investigation, formal analysis, visualization, writing – original draft. Oluwagbemiga P. Ojo: formal analysis, visualization. George S. Nolas: conceptualization, investigation, supervision, writing – review & editing, project administration.

Conflicts of interest

There are no conflicts to declare.

Notes and references

1 E. S. Toberer, L. L. Baranowski and C. Dames, Annu. Rev. Mater. Res., 2012, 42, 179–209.
2 B. Liu, Y. Liu, C. Zhu, H. Xiang, H. Chen, L. Sun, Y. Gao and Y. Zhou, J. Mater. Sci. Technol., 2019, 35, 833–851.
3 C. Chang and L.-D. Zhao, Mater. Today Phys., 2018, 4, 50–57.
4 T. Ghosh, M. Dutta, D. Sarkar and K. Biswas, J. Am. Chem. Soc., 2022, 144, 10099–10118.
5 H. A. Eivari, Z. Sohbatzadeh, P. Mele and M. H. N. Assadi, Mater. Today Energy, 2021, 21, 100744.
6 P. G. Klemens and M. Gell, Mater. Sci. Eng. A, 1998, 245, 143–149.
7 D. R. Clarke, Surf. Coat. Technol., 2003, 163–164, 67–74.
8 R. E. Taylor, Mater. Sci. Eng. A, 1998, 245, 160–167.

9 R. Vassen, A. Stuke and D. Stöver, J. Therm. Spray Technol., 2009, 18, 181–186.
10 J. R. Nicholls, K. J. Lawson, A. Johnstone and D. S. Rickerby, Surf. Coat. Technol., 2002, 151–152, 383–391.
11 M. Wuttig and N. Yamada, Nat. Mater., 2007, 6, 824–832.
12 T. Yamamoto, S. Hatayama and Y. Sutou, Int. J. Mater. Eng. Appl., DOI:10.1016/j.matdes.2022.110560.
13 A. A. Rockett, Curr. Opin. Solid State Mater. Sci., 2010, 14, 143–148.
14 Q. Cao, O. Gunawan, M. Copel, K. B. Reuter, S. J. Chey, V. R. Deline and D. B. Mitzi, Adv. Energy Mater., 2011, 1, 845–853.
15 T. Todorov and D. B. Mitzi, Eur. J. Inorg. Chem., 2010, 2010, 17–28.
16 S. Palchoudhury, K. Ramasamy and A. Gupta, Nanoscale Adv., 2020, 2, 3069–3082.
17 W. Wang, M. T. Winkler, O. Gunawan, T. Gokmen, T. K. Todorov, Y. Zhu and D. B. Mitzi, Adv. Energy Mater., 2014, 4, 1301465.
18 A. H. A. Al-Waeli, H. A. Kazem, M. T. Chaichan and K. Sopian, Int. J. Energy Res., 2021, 45, 1269–1308.
19 N. F. M. Razali, A. Fudholi, M. H. Ruslan and K. Sopian, Int. J. Electr. Comput. Eng. IJECE, 2019, 9, 134.
20 Y. Dong, A. R. Khabibullin, K. Wei, J. R. Salvador, G. S. Nolas and L. M. Woods, ChemPhysChem, 2015, 16, 3264–3270.
21 Y. Dong, H. Wang and G. S. Nolas, Phys. Status Solidi RRL – Rapid Res. Lett., 2014, 8, 61–64.
22 Y. Dong, H. Wang and G. S. Nolas, Inorg. Chem., 2013, 52, 14364–14367.
23 K. Wei, L. Beauchemin, H. Wang, W. D. Porter, J. Martin and G. S. Nolas, J. Alloys Compd., 2015, 650, 844–847.
24 O. P. Ojo, W. D. C. B. Gunatilleke, H. Wang and G. S. Nolas, Dalton Trans., 2022, 51, 6220–6225.
25 T.-R. Wei, P. Qiu, K. Zhao, X. Shi and L. Chen, Adv. Mater., 2023, 35, 2110236.
26 W. D. C. B. Gunatilleke, R. Juneja, O. P. Ojo, A. F. May, H. Wang, L. Lindsay and G. S. Nolas, Phys. Rev. Mater., 2021, 5, 085002.
27 M. T. Agne, T. Böger, T. Bernges and W. G. Zeier, PRX Energy, 2022, 1, 031002.
28 C.-W. Wu, X. Ren, W.-X. Zhou, G. Xie and G. Zhang, APL Mater., 2022, 10, 040902.
29 A. M. Bates, Y. Preger, L. Torres-Castro, K. L. Harrison, S. J. Harris and J. Hewson, Joule, 2022, 6, 742–755.
30 X. Yu, R. Chen, L. Gan, H. Li and L. Chen, Engineering, 2023, 21, 9–14.
31 T. Krauskopf, S. Muy, S. P. Culver, S. Ohno, O. Delaire, Y. Shao-Horn and W. G. Zeier, J. Am. Chem. Soc., 2018, 140, 14464–14473.
32 J. Liang, X. Li, K. R. Adair and X. Sun, Acc. Chem. Res., 2021, 54, 1023–1033.
33 Y. Kato, S. Hori, T. Saito, K. Suzuki, M. Hirayama, A. Mitsui, M. Yonemura, H. Iba and R. Kanno, Nat. Energy, 2016, 1, 1–7.
34 J. Ding, J. L. Niedziela, D. Bansal, J. Wang, X. He, A. F. May, G. Ehlers, D. L. Abernathy, A. Said, A. Alatas, Y. Ren, G. Arya and O. Delaire, Proc. Natl. Acad. Sci., 2020, 117, 3930–3937.
35 J. L. Niedziela, D. Bansal, A. F. May, J. Ding, T. Lanigan-Atkins, G. Ehlers, D. L. Abernathy, A. Said and O. Delaire, Nat. Phys., 2019, 15, 73–78.
36 B. Jiang, P. Qiu, H. Chen, Q. Zhang, K. Zhao, D. Ren, X. Shi and L. Chen, Chem. Commun., 2017, 53, 11658–11661.
37 S. Ohno, A. Banik, G. F. Dewald, M. A. Kraft, T. Krauskopf, N. Minafra, P. Till, M. Weiss and W. G. Zeier, Prog. Energy, 2020, 2, 022001.
38 B. Li, H. Wang, Y. Kawakita, Q. Zhang, M. Feygenson, H. L. Yu, D. Wu, K. Ohara, T. Kikuchi, K. Shibata, T. Yamada, X. K. Ning, Y. Chen, J. Q. He, D. Vaknin, R. Q. Wu, K. Nakajima and M. G. Kanatzidis, Nat. Mater., 2018, 17, 226–230.
39 P. Simonnin, M. Sassi, B. Gilbert, L. Charlet and K. M. Rosso, J. Phys. Chem. C, 2020, 124, 10150–10158.
40 T. Bernges, R. Hanus, B. Wankmiller, K. Imasato, S. Lin, M. Ghidiu, M. Gerlitz, M. Peterlechner, S. Graham, G. Hautier, Y. Pei, M. R. Hansen, G. Wilde, G. J. Snyder, J. George, M. T. Agne and W. G. Zeier, Adv. Energy Mater., 2022, 12, 2200717.
41 M. K. Gupta, J. Ding, D. Bansal, D. L. Abernathy, G. Ehlers, N. C. Osti, W. G. Zeier and O. Delaire, Adv. Energy Mater., 2022, 12, 2200596.
42 F. Damay, S. Petit, S. Rols, M. Braendlein, R. Daou, E. Elkaïm, F. Fauth, F. Gascoin, C. Martin and A. Maignan, Sci. Rep., 2016, 6, 23415.
43 Z. Cheng, B. Zahiri, X. Ji, C. Chen, D. Chalise, P. V. Braun and D. G. Cahill, Small, 2021, 17, 2101693.
44 P. C. Harikesh, A. Surendran, B. Ghosh, R. A. John, A. Moorthy, N. Yantara, T. Salim, K. Thirumal, W. L. Leong, S. Mhaisalkar and N. Mathews, Adv. Mater., 2020, 32, 1906976.
45 W. W. Winnie Leung, C. N. Savory, R. G. Palgrave and D. O. Scanlon, J. Mater. Chem. C, 2019, 7, 2059–2067.
46 W.-C. Sun, S. U. Rahayu and M.-W. Lee, IEEE J. Photovolt., 2018, 8, 1011–1016.
47 S. U. Rahayu, C.-L. Chou, N. Suriyawong, B. A. Aragaw, J.-B. Shi and M.-W. Lee, APL Mater., 2016, 4, 116103.
48 X. Zhang, M. Huang, P. Xu, C.-M. Dai, Z.-H. Cai, D. Han and S. Chen, Prog. Nat. Sci. Mater. Int., 2019, 29, 322–328.
49 J. Martin and G. S. Nolas, Rev. Sci. Instrum., 2016, 87, 015105.
50 J. Martin, S. Erickson, G. S. Nolas, P. Alboni, T. M. Tritt and J. Yang, J. Appl. Phys., 2006, 99, 044903.
51 T. K. Bera, J. I. Jang, J.-H. Song, C. D. Malliakas, A. J. Freeman, J. B. Ketterson and M. G. Kanatzidis, J. Am. Chem. Soc., 2010, 132, 3484–3495.
52 X. Hua, V. I. Hegde and C. Wolverton, Chem. Mater., 2019, 31, 9445–9452.
53 Z. Xia, F.-X. Yu, S.-C. Lu, D.-J. Xue, Y.-S. He, B. Yang, C. Wang, R.-Q. Ding, J. Zhong and J. Tang, Chin. Chem. Lett., 2017, 28, 881–887.
54 C. Kittel and P. McEuen, Introduction to Solid State Physics, John Wiley & Sons, 2018.
55 M. T. Agne, R. Hanus and G. Jeffrey Snyder, Energy Environ. Sci., 2018, 11, 609–616.
56 J. Callaway, Phys. Rev., 1959, 113, 1046–1051.
57 Y. He, T. Day, T. Zhang, H. Liu, X. Shi, L. Chen and G. J. Snyder, Adv. Mater., 2014, 26, 3974–3978.
58 K. S. Weldert, W. G. Zeier, T. W. Day, M. Panthöfer, G. J. Snyder and W. Tremel, J. Am. Chem. Soc., 2014, 136, 12035–12040.
59 T. M. Tritt, Thermal Conductivity: Theory, Properties, and Applications, Springer Science & Business Media, 2005.
60 G. Krenzer, C.-E. Kim, K. Tolborg, B. J. Morgan and A. Walsh, J. Mater. Chem. A, 2022, 10, 2295–2304.
61 T. M. Brenner, C. Gehrmann, R. Korobko, T. Livneh, D. A. Egger and O. Yaffe, Phys. Rev. Mater., 2020, 4, 115402.…